Global phase diagram of competing ordered and quantum spin-liquid phases on the kagome lattice

Shou-Shu Gong, Wei Zhu, Leon Balents, and D. N. Sheng

Phys. Rev. B **91**, 075112 — Published 17 February 2015

DOI: 10.1103/PhysRevB.91.075112

Global Phase Diagram of Competing Ordered and Quantum Spin Liquid Phases on the Kagomé Lattice

Shou-Shu Gong[1], Wei Zhu[1], Leon Balents[2], and D. N. Sheng[1]
[1]*Department of Physics and Astronomy, California State University, Northridge, California 91330, USA*
[2]*Kavli Institute for Theoretical Physics, University of California, Santa Barbara, California 93106-4030, USA*

We study the quantum phase diagram of the spin-$1/2$ Heisenberg model on the kagomé lattice with first-, second-, and third-neighbor interactions J_1, J_2, and J_3 by means of density matrix renormalization group. For small J_2 and J_3, this model sustains a time-reversal invariant quantum spin liquid phase. With increasing J_2 and J_3, we find in addition a $q = (0, 0)$ Néel phase, a chiral spin liquid phase, an apparent valence-bond crystal phase, and a complex non-coplanar magnetically ordered state with spins forming the vertices of a cuboctahedron known as a *cuboc1* phase. Both the chiral spin liquid and *cuboc1* phase break time reversal symmetry in the sense of spontaneous scalar spin chirality. We show that the chiralities in the chiral spin liquid and *cuboc1* are distinct, and that these two states are separated by a strong first order phase transition. The transitions from the chiral spin liquid to both the $q = (0, 0)$ phase and to time-reversal symmetric spin liquid, however, are consistent with continuous quantum phase transitions.

PACS numbers: 73.43.Nq, 75.10.Jm, 75.10.Kt

I. INTRODUCTION

Quantum spin liquids (QSLs) are highly entangled states of matter[1] with remarkable properties of great intrinsic interest. The simplest and perhaps most striking subclass of QSLs comprises topologically ordered states[2–4], which have a non-vanishing excitation gap, and support emergent quasiparticles with anyonic statistics and fractional quantum numbers[5–9]. Although QSLs have been demonstrated in many contrived models[10–17], their relation to magnetically disordered phases in different frustrated systems remains poorly understood. This problem has been intensively studied in the past by many theoretical approaches.

Apart from their intrinsic interest, motivation to understand QSL phases comes from recent experimental discoveries. The kagomé antiferromagnets herbertsmithite and kapellasite have recently emerged as prominent examples[18–24]. The absence of magnetic order is evidenced by many different techniques including muon spin rotation and susceptibility measurements[18–24], and neutron scattering measurements of herbertsmithite show a purely continuum spectrum, interpreted as a signature of fractional "spinon" excitations[23]. Further instances of QSLs have been found in organic Mott insulators with a triangular lattice structure[25–27].

Theoretically, QSLs have been sought in spin-$1/2$ antiferromagnets with frustrated and/or competing interactions on triangular[28–31], honeycomb[32–36], square[37–39], and kagomé[40–44] lattices. Amongst all these, the kagomé Heisenberg model (KHM) appears to possess the most robust QSL phase, and the only one consistently found in unbiased density matrix renormalization group (DMRG) calculations. The nature of the QSL is less clear. The DMRG studies suggest a gapped QSL[40–43], seemingly consistent with Z_2 topological order[42,43]. Variational studies using projected fermionic parton wavefunctions favor a different, gapless Dirac state[45–47]. A bosonic parton wavefunction does, however, give a competitive energy for a Z_2 QSL state in the extended J_1-J_2 KHM with second-neighbor antiferromagnetic exchange J_2[48], and other studies reinforce an enhanced QSL phase in this model[43,49–51]. Direct evidence for Z_2 topological order is mixed: in support, a nearly quantized topological entanglement entropy was found in the J_1-J_2 model[43], but the expected four topological ground state sectors have not been seen in DMRG[52].

Interestingly, by introducing *both* second and third neighbor couplings, DMRG studies[53–56] recently discovered another topological QSL on the kagomé lattice. This state spontaneously breaks time reversal symmetry (TRS) in the sense of having a complex wavefunction and non-zero scalar spin chirality $\chi_{ijk} = S_i \cdot (S_j \times S_k)$ for some triplets of nearby spins i, j, k. Such a state, proposed more than 20 years ago by Kalmeyer and Laughlin[57,58], is known as a Chiral Spin Liquid (CSL). It can be regarded as a spontaneous fractional quantum Hall effect. The CSL occurs in several different kagomé spin models with comparable J_2 and J_3[53,59,60] or chiral interactions[61], and indeed is *more* robust than the putative Z_2 QSL state discussed earlier: all the expected universal topological properties of the CSL state have been verified numerically.

In this paper, we expose the relations between the two QSL states and nearby ordered phases through a global DMRG[62] study of the full phase diagram of the J_1-J_2-J_3 model (with all exchanges antiferromagnetic):

$$H = J_1 \sum_{\langle i,j\rangle} S_i \cdot S_j + J_2 \sum_{\langle\langle i,j\rangle\rangle} S_i \cdot S_j + J_3 \sum_{\langle\langle\langle i,j\rangle\rangle\rangle} S_i \cdot S_j. \quad (1)$$

Good points of comparison are the classical and Schwinger boson mean field phase diagrams, found in Ref. 63. These studies found two magnetically ordered phases breaking TRS, known as *cuboc1* and *cuboc2*, as well as a simpler $q = (0, 0)$ coplanar ordered state which is time-reversal symmetric. They also conjectured that a Z_2 TRS breaking QSL "descended" from the *cuboc1* state by quantum disordering of the spins might apply to the the pure nearest-neighbor KHM, and also extend to the region with small J_2 and J_3 perturbations[63]. The DMRG phase diagram determined here is shown in Fig. 1(a), and bears out some but not all of these

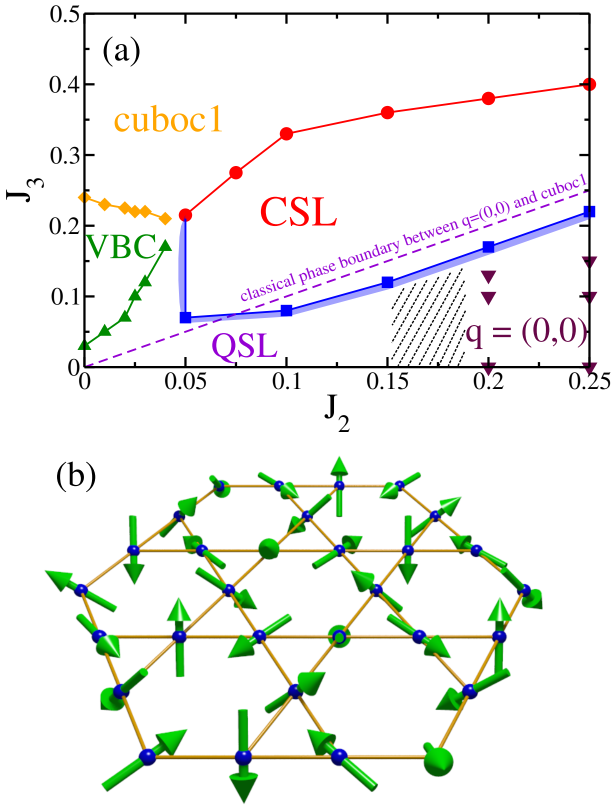

FIG. 1: (a) Quantum phase diagram of the spin-1/2 J_1-J_2-J_3 kagomé Heisenberg model for $0.0 \leq J_2 \leq 0.25$ and $0.0 \leq J_3 \leq 0.5$. The phases shown are: a time-reversal invariant quantum spin liquid (QSL) phase, a coplanar magnetically ordered $q = (0, 0)$ Néel phase, a time-reversal broken chiral spin liquid (CSL) phase, a non-coplanar magnetically and chiral ordered *cuboc1* phase, and a valence bond crystal (VBC) phase. The *cuboc1* phase remains stable for larger J_3 beyond the range shown here (we have checked up to $J_3 \leq 1.0$). The dashed region indicates the uncertainty in locating the phase boundary between the QSL and $q = (0, 0)$ Néel phases. The purple dashed line shows the line of classical degeneracy between the $q = (0, 0)$ Néel and *cuboc1* phases[63]. (b) The configurations of spins (arrows indicate the direction of static moments) of the *cuboc1* state on the kagomé lattice. On each small triangle, the spins are coplanar and sum to zero. In each hexagon, sets of three consecutive spins are non-coplanar, as are the sets obtained by taking every second spin around the hexagon. This breaks time-reversal symmetry in the sense that the scalar spin chirality is non-zero and the wavefunction is intrinsically complex.

features. We indeed find the ordered *cuboc1* (see Fig. 1(b) of the spin configuration of *cuboc1* state) and $q = (0, 0)$ states when J_3 or J_2 are large, roughly correlating with their classical positions. These classical states surround three more quantum ones: the two aforementioned QSL states and a third state tentatively identified as a Valence Bond Crystal (VBC) state, which breaks translational but not spin-rotation or TRS symmetry. The relations between the spin liquid states and the classical ones will be discussed below. We do not focus on the VBC phase here, but make a few remarks upon it in Sec. VI.

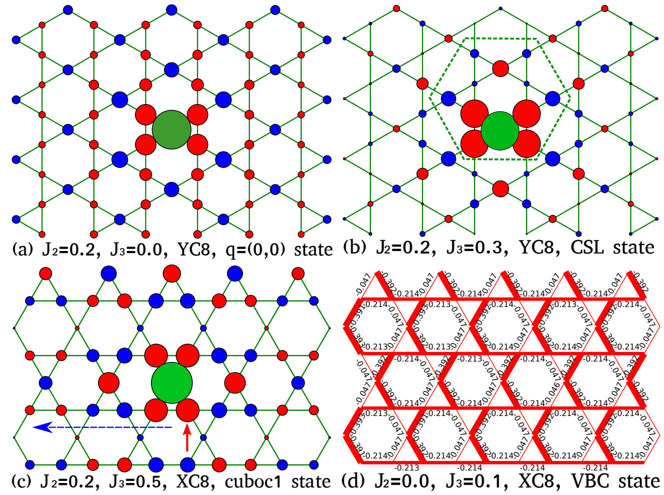

FIG. 2: (a)-(c) show the spin-spin correlations for different phases on the YC8 and XC8 cylinders. The green site is the reference spin, the blue and red colors denote positive and negative correlations, respectively, of the site in question with the reference spin. The area of circle is proportional to the magnitude of the spin correlation. The large dashed hexagon in (b) shows the short-range spin correlations in CSL phase. The arrows in (c) show the reference spin (the red solid arrow) and the direction of other spins (the blue dashed arrow) whose correlations are plotted in Fig. 3. Panel (d) plots the nearest-neighbor bond energy on the XC8 cylinder in the VBC phase.

For this study, we use the DMRG with $SU(2)$ spin rotational symmetry[64] on cylinders by keeping a number of $U(1)$-equivalent states M as large as $M_{\max} = 26000$. Two cylinder geometries, denoted XC and YC, are used, such that for the XC (YC) cylinder, one of the three bond orientations is along the x (y) axis, as shown in Fig. 2. We abbreviate specific cylinders by XC$2L_y$-L_x and YC$2L_y$-L_x, where L_x (L_y) is the number of unit cells in the x (y) direction. In general, we obtain results with DMRG truncation error less than 1×10^{-6} and 1×10^{-5} for the cylinders with $L_y = 4$ and 6, respectively.

II. $q = (0, 0)$ NÉEL PHASE IN THE J_1-J_2 KHM

We begin by studying the $q = (0, 0)$ Néel order in the small J_2 region with $J_3 = 0$, and first investigate the spin correlations on cylinders of varying widths. A gapped magnetically disordered phase would be expected to show exponentially decaying correlations. In a long-range magnetically ordered phase, the correlations should remain non-zero in magnitude at long distances *in two dimensions*. On a long cylinder of even width, exponential decay is still expected even when the two dimensional limit is ordered, but in that case the decay is characterized by a correlation length ξ which grows linearly with system width. Thus it is crucial to investigate the scaling of the correlation length.

Fig. 3(a) shows the correlations between spins on the same sublattice, $\langle S_0 \cdot S_d \rangle$, on the XC8-24 cylinder. One sees that the spin correlation length continues to grow with increasing

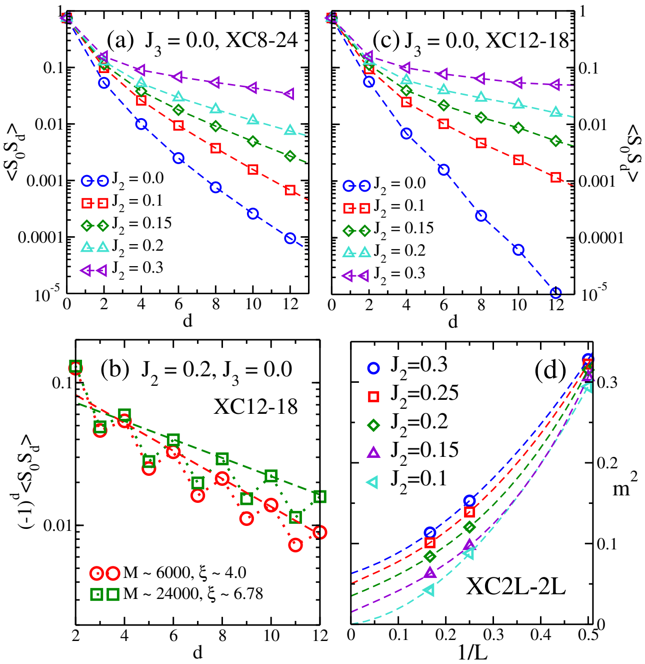

FIG. 3: Panels (a) and (c) are log-linear plots of the spin correlations between sites of one sublattice versus site distance d on the XC8 and XC12 cylinders. Panel (b) illustrates the dependence upon the number of states kept, M, in the DMRG, for the case $J_2 = 0.2$ on the XC12 cylinder. The geometry of the sites in the first three panels is shown in Fig. 2(c). Panel (d) shows the finite size scaling of the (squared) magnetic order parameter m^2 versus $1/L$ on the XC4, XC8, and XC12 cylinders using the fitting formula $m^2(1/L) = m^2(1/L = 0) + a/L + b/L^2$. All plots in this figure are for $J_3 = 0$.

J_2. At $J_2 = 0.2$, the system appears to develop longer-range correlation. While the results on the XC8 cylinder are fully converged, those on the wider XC12 cylinder are not, and display dependence on the number of states kept in DMRG. In particular, ξ grows as more states are included. Therefore we measure the spin correlations for several different numbers, $M = 4000 - 24000$, of $U(1)$-equivalent states and extrapolate the result. For example at $J_2 = 0.2$ (shown in Fig. 3(b)), ξ is 4.0 lattice spacings for $M \approx 6000$ states while it grows to 6.78 lattice spacings when $M \approx 24000$ states. Thus, the less converged results may underestimate Néel order. In Fig. 3(c), we show the spin correlations on the XC12 cylinder obtained with $M \approx 24000$ states. Comparing to Fig. 3(a), we observe that for $J_2 = 0$, the correlation length *decreases* with cylinder width, while it *increases* with width for $J_2 = 0.1 - 0.2$. The trend is at least indicative of growing order.

Next, we study the J_2 dependence of the magnetic order parameter, extrapolating to the thermodynamic limit from finite-size systems. We calculate the finite-size order parameter from the middle half of each system to minimize boundary effects, i.e. the $3\times L\times L$ sites out of a total of $3\times L\times 2L$ sites for the XC$2L$-$2L$ ($L = 2, 4, 6$) cylinders. The order parameter of the $q = (0, 0)$ Néel state is defined as $m^2 = \frac{1}{N^2}\sum_{i,j}\langle S_i \cdot S_j\rangle$ (N is the number of unit cells, and i, j are sites in the same sublattice). In Fig. 3(d), we show m^2 versus $1/L$ for various J_2[65]. For $J_2 \geq 0.15$, we find that m^2 extrapolates to finite values in the thermodynamic limit, indicative of $q = (0, 0)$ Néel long range order. Because of the limited range of system width, we have considerable uncertainty in the location of the phase boundary and cannot reliably estimate an error bar. However, we feel confident that the magnetic order is robust for $J_2 = 0.2$, as shown in Fig. 3(b-c), which sets a lower bound on the transition point.

III. CHIRAL SPIN LIQUID PHASE

Prior work has fully established the CSL state in the J_1-J_2-J_3 KHM along the parameter line $J_2 = J_3 = J'$ with $0.1 \lesssim J' \lesssim 0.7$[53]. Moreover, the topological order of the CSL was found to be that of the $\nu = 1/2$ Laughlin state[53]. This completely fixes the universal topological aspects of the CSL. Here we study some non-universal aspects of the CSL which help to show its relation to the surrounding phases. First, we determine the complete domain of the CSL phase through a study of the scalar spin chirality. In Fig. 4(a), we show the correlation function between chirality on pairs of the smallest triangles of the kagomé lattice (indicated with the number "1" in the inset of Fig. 4(b)), for the YC8-24 cylinder with $J_2 = 0.2$ and various J_3. In the $q = (0, 0)$ Néel phase, for example for $J_3 = 0.1$, the chiral correlations decay rapidly and exponentially to zero. With increasing J_3, the chiral correlations gradually grow, apparently establishing long-range order (i.e. saturating to a finite value at large distance) at $J_3 \simeq 0.22$. This behavior persists to $J_3 \simeq 0.4$, beyond which the chiral correlations exhibit a sharp decrease. We define χ as the square root of the long-distance chiral correlations in Fig. 4(a) $\chi \equiv \sqrt{|\langle\chi_0\chi_d\rangle|}$ (d is the longest available distance) to describe the variation of chiral correlation. Fig. 4(b) shows the J_3 dependence of χ, which clearly indicates the CSL phase exists over a well-defined but limited range of J_3. From this figure, we conservatively estimate $\chi = 0$ for $J_3 \lesssim 0.2$ and $J_3 \gtrsim 0.4$. We note that chiral order, which breaks the discrete Z_2 time reverse symmetry, can exist even in a one-dimensional system. So we must carefully consider the behavior on wider cylinders to firmly establish the presence of chiral order in *two* dimensions. To do so, we compare the behavior on the YC8 cylinder to that on XC12 and YC12 cylinders, as in Figs. 4(c) and 4(d). We see that for some exchange parameters, the chiral order grows *stronger* with increasing system width, which we take as evidence for time-reversal symmetry breaking in two dimensions. Using this behavior as a first criterion for the CSL, and the second that magnetic correlations are short-ranged, we arrive at the shaded boundary between the $q = (0, 0)$ Néel phase and the CSL shown in Fig. 1(a).

To further reveal the structure of the chirality in the CSL, we study the chiral correlations between pairs of triangles of each of the four types shown in the inset of Fig. 4(b). Results for $J_2 = 0.2, J_3 = 0.24$ on YC8-24 and YC12-24 cylinders are shown in Figs. 4(c) and 4(d). Clearly correlations of all four types of triangles have long-range order, which

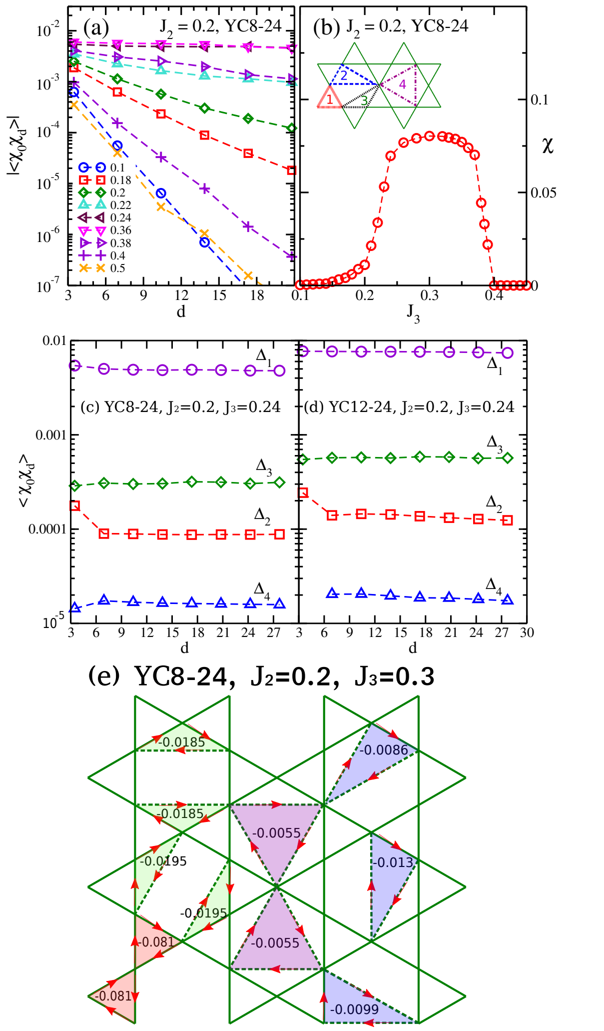

FIG. 4: Numerical results for scalar spin chirality. Panel (a) shows correlations between pairs of the smallest triangles Δ_1 on the kagomé lattice for $J_2 = 0.2$ and different values of J_3 on the YC8-24 cylinder. In (b), the long-distance value of these correlations is extracted and plotted versus J_3, which clearly shows the CSL region. Plots (c) and (d) compares the correlations of different types of triangles (defined in the inset of (b)) for $J_2 = 0.2, J_3 = 0.24$ on the YC8-24 and YC12-24 cylinders. Panel (e) shows the chiral order parameter $\langle \chi_{\Delta_i} \rangle$ calculated directly from the complex code for the indicated triangles on the YC8-24 cylinder at $J_2 = 0.2, J_3 = 0.3$. The red arrows indicate the order of the three spins in the triple product defining the scalar spin chirality.

demonstrates spontaneous scalar spin chirality on all triangles. The largest chirality occurs on the smallest triangles (labeled Δ_1). As a check, we also calculate the expectation value of the local scalar spin chirality directly using a complex code, which allows broken time-reversal symmetry. The results for the YC8-24 cylinder at $J_2 = 0.2, J_3 = 0.3$ are shown in Fig. 4(e). We see that the expectation values are indeed all non-zero and of a uniform sign. Moreover the magnitudes of the spontaneous spin chirality obtained in this way obey $|\langle \chi_{\Delta_1} \rangle| > |\langle \chi_{\Delta_3} \rangle| > |\langle \chi_{\Delta_2} \rangle| > |\langle \chi_{\Delta_4} \rangle|$, consistent with the

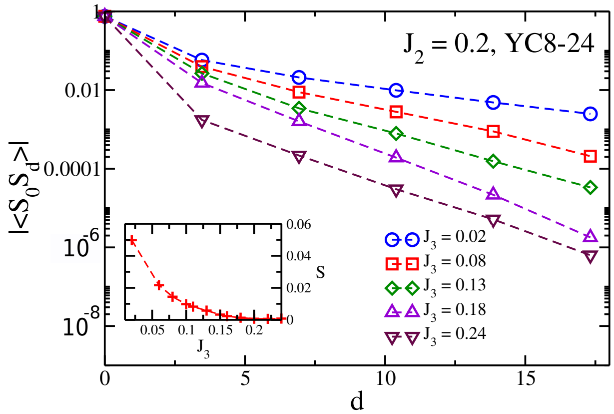

FIG. 5: Log-linear plot of spin correlations for $J_2 = 0.2$ on the YC8-24 cylinder. These correlations decay more quickly with J_3 – a consequence of the transition from the $q = (0, 0)$ Néel to the CSL phase. This is seen more clearly from the plot of the long-distance spin correlation S versus J_3, shown in the inset.

results of the correlation function analysis. We note that, up to very small discrepancies which we attribute to the boundary effects due to the cylinder geometry, the spontaneous chiralities respect the translational and rotational symmetries of the lattice.

Finally, we consider the spin correlations on passing between the $q = (0, 0)$ phase and the CSL state. We take $J_2 = 0.2$ as an example – see Fig. 5. When J_3 is small, the system is in the $q = (0, 0)$ phase and the spin correlations are large and slowly decaying with a correlation length that grows with system width. With increasing J_3, the spin correlations decrease gradually. We define the long-distance spin correlation $S \equiv \sqrt{|\langle S_0 \cdot S_d \rangle|}$ (d is the longest distance) as a crude estimate of magnetic order. The inset of Fig. 5 shows the J_3 dependence of S, which decreases rather smoothly and for practical purposes vanishes around $J_3 = 0.2$. This corresponds to the onset of the CSL phase. For larger J_3, the short range $q = (0, 0)$ spin correlation pattern is destroyed and the system shows instead a pattern of spin correlations which at short distances is consistent with that of the *cuboc1* state. One such an example for $J_2 = 0.2, J_3 = 0.3$ is shown in Fig. 2(b).

IV. *CUBOC1* PHASE

The *cuboc1* state was first proposed for a kagomé antiferromagnet in an exact diagonalization study of the J_1-J_3 KHM for $J_3 \gtrsim 0.25$[66]. It is characterized by a 12-sublattice non-coplanar magnetic ordering in which the spins point towards the corners of a cuboctahedron (see Fig. 1(b)), one of the archimedean solids[63]. In the classical J_1-J_2-J_3 KHM, the *cuboc1* phase occurs for $J_3 > J_2$ ($J_2 < 1.0$), and shares a direct phase boundary with the $q = (0, 0)$ Néel phase as shown in Fig. 1(a)[63]. Owing to its non-coplanarity, the *cuboc1* state breaks time-reversal symmetry and it is natural therefore to imagine it may be the classical ancestor of a CSL state. Here we investigate this possibility in more detail, and argue that the CSL in the KHM is *not* the descendent of the *cuboc1* state.

We first however verify the magnetic order of the *cuboc1* state by studying the spin-spin correlation function. The spin correlation pattern is, in sign and magnitude, consistent with the *cuboc1* state for several cylindrical geometries, provided they are chosen compatible with the enlarged unit cell of this state. An example is shown in Fig. 6(a), where a *cuboc1* pattern with a 12-site unit cell indicated by the dashed hexagon is clearly seen. A characteristic feature is that the spin correlations in the columns denoted by the red arrows are small and decay quickly. This follows naturally from the classical picture of the *cuboc1* state, because these spins are perpendicular to the reference spin.

To quantify the magnetic ordering, we study the evolution of the spin correlations with increasing J_3. An example is shown in Fig. 6(b) for $J_2 = 0.2$, $0.24 \leq J_3 \leq 0.5$ on the YC8-24 cylinder. One sees that the spin correlations decay quite fast for $J_3 < 0.4$, consistent with the gapped CSL shown in Fig. 4(b). At $J_3 = 0.4$, the spin correlations are sharply enhanced and approach finite values at long distance for $J_3 > 0.4$. We define S as the square root of the long-distance spin correlations in Fig. 6(b) $S \equiv \sqrt{|\langle S_0 \cdot S_d \rangle|}$ (d is the longest distance), and plot it versus J_3 in the inset, which shows a jump of S from zero to a finite value at $J_3 \simeq 0.4$. The abrupt simultaneous onset of spin order and vanishing chiral order on small triangles (Fig. 4(b)), together indicate a phase transition from the CSL to a magnetically ordered phase.

To be fully confident of magnetic ordering, we must consider finite size effects. We compare the spin correlations on YC8 and YC12 cylinders (the XC12 cylinder is incompatible with *cuboc1* state). Interestingly, the *cuboc1* state has significantly enhanced entanglement entropy – a point which we return to below – which prevents us from obtaining fully converged results on YC12 cylinder. Therefore, we instead compare the spin correlations on the YC8 and YC12 cylinders as obtained with similar truncation errors. As shown in Figs. 6(c) and 6(d) for $J_2 = 0.2, J_3 = 0.5$, the spin correlations grow with decreasing truncation error (increasing M) in both systems. For similar truncation errors, the correlation length ξ on the wider YC12 cylinder is always larger than that on the YC8 cylinder. Consequently, the converged spin correlations (obtained from extrapolation with respect to truncation error, as shown by the plus symbol) on the YC12 cylinder are stronger than those on the YC8 cylinder. The growing spin correlation length is consistent with the presence of magnetic order in two-dimensional thermodynamic limit.

Now we justify the claim that the CSL *cannot* be regarded as a quantum fluctuating *cuboc1* state. To see this, we first consider the pattern of scalar spin chirality in the *cuboc1* state. Classically, the spins in triangles Δ_1 and Δ_2 are *coplanar*, so these possess zero scalar spin chirality. Spin chirality is instead concentrated in triangles Δ_3 and Δ_4, where the spins are non-coplanar[63]. We indeed see precisely this behavior in the numerical calculations of chirality correlations, which are large and consistent with long-range chiral order *only* for triangles Δ_3 and Δ_4, as shown in Fig. 6(e). This is why the chirality calculated for the small (Δ_1) triangles in Fig. 4(b) jumps to zero in the *cuboc1* state. In Fig. 6(e), we see some

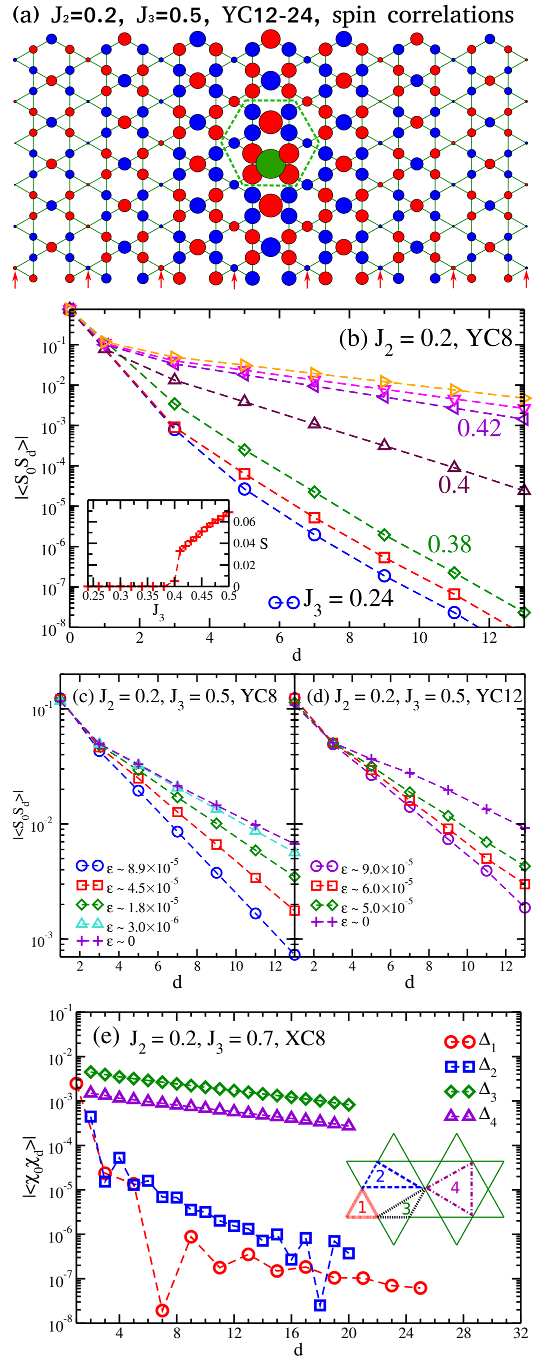

FIG. 6: Numerical studies of the *cuboc1* phase. All plots in this figure use $J_2 = 0.2$. In (a) we show the spin correlations for a central region of the YC12-24 cylinder with $J_3 = 0.5$, following the same conventions as Fig. 2. The dashed hexagon indicates the 12-site unit cell. Panel (b) shows log-linear plots of the spin correlations for various J_3 values on the YC8-24 cylinder (here $J_3 = 0.24, 0.3, 0.38, 0.4, 0.42, 0.45, 0.5$ for the successive curves with increasing values of the correlations). The inset plots the J_3 dependence of the long-distance spin correlation S. Plots (c) and (d) compare the spin correlation for $J_3 = 0.5$ on the YC8-24 and YC12-24 cylinders with different truncation errors ε. The data with plus symbol give the results of an extrapolation to zero truncation error. Panel (e) contrasts the correlations of the chirality on the four different types of triangles (as shown in the inset) well into the *cuboc1* phase for $J_3 = 0.7$ on the XC8-24 cylinder. The correlations on the Δ_1, Δ_2 triangles are very small and sometimes change sign. This is probably consistent with zero spontaneous chirality on these triangles in the thermodynamic limit.

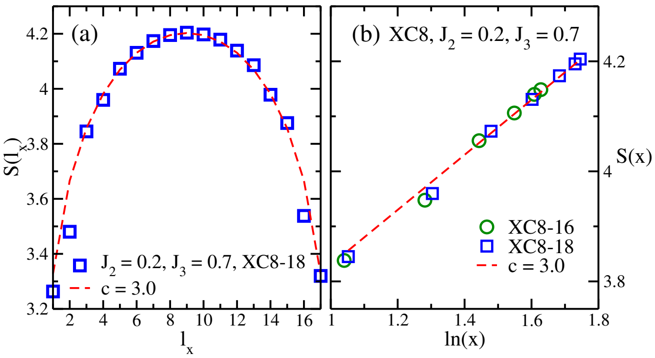

FIG. 7: Entanglement entropy in the *cuboc1* phase. In (a) the entanglement entropy versus the sub-system length l_x for $J_2 = 0.2$, $J_3 = 0.7$ on the XC8-18 cylinder is fitted using the conformal field theory formula $S(l_x) = (c/6)\ln[(L_x/\pi)\sin(l_x\pi/L_x))] + g$ with $c = 3.0, g = 3.3$. In (b), the entanglement entropy is plotted versus $\ln x$ ($x = (L_x/\pi)\sin(l_x\pi/L_x)$) for $J_2 = 0.2$, $J_3 = 0.7$ on XC8-16 and XC8-18 cylinders. The dashed line is the fit curve used shown in (a).

very small residual chirality correlations on the type 1 and 2 triangles, but these are consistent with short-range correlations, which are always non-zero and do not indicate symmetry breaking. The absence of scalar spin chirality in the small triangles in the *cuboc1* state reflects an invariance of this state under a combined C_2 rotation in spin space (about an axis through two antipodal points on the cuboctahedron) and a real space reflection through a plane bisecting a column of small triangles. The CSL state breaks this symmetry. Hence the two phases are *symmetry distinct* even beyond the presence of spin ordering.

Finally, we return to the entanglement entropy in the *cuboc1* state. The large entropy may be understood from general arguments. In the two-dimensional limit, the *cuboc1* phase fully breaks SU(2) spin symmetry, and so has *three* gapless Goldstone modes (a number equals to the number of generators of SU(2)). This is described field-theoretically by an 2+1-dimensional SO(3) matrix non-linear sigma model[67]. If we now imagine placing the *cuboc1* state on a (compatible) cylinder, the momentum along the circumferential direction k_y becomes quantized, and we naïvely expect three gapless one-dimensional bosonic modes with $k_y = 0$. In general, these modes are interacting, and for long cylinders fluctuate strongly and are expected to open up a gap, since the non-linear sigma model in 1+1-dimensions is asymptotically free. However, this gap is exponentially small when the cylinder circumference is large, and so we can expect a wide regime in which the cylinder behaves like a system of *three* gapless free bosonic modes.

For a general free gapless bosonic system (actually any conformal field theory) in 1+1-dimensions, the entanglement entropy of a bipartition into two halves follows the area law $S(l_x) = (c/6)\ln[(L_x/\pi)\sin(l_x\pi/L_x))] + g$[68], where c is the characteristic central charge of system, g is a nonuniversal constant reflecting short-range entanglement, and l_x and L_x are the length of subsystem and the whole system, respectively. The non-linear sigma model argument above implies $c = 3$. Thus the large entanglement entropy of the *cuboc1* state on cylinders could be attributed to its Goldstone mode structure.

We verify this numerically in more detail, and find behavior consistent with this prediction. An example of the l_x dependence of entropy is shown in Fig. 7(a) for $J_2 = 0.2, J_3 = 0.7$ on the XC8-18 cylinder. We bipartition the system column by column, and denote the number of columns as l_x. The entropy fits quite well using the area law behavior with $c = 3.0, g = 3.3$. In Fig. 7(b), we plot the same data versus $\ln[(L_x/\pi)\sin(l_x\pi/L_x))]$, where the slope of the dashed line determines the central charge. We find that the entropy on XC8-16 cylinder also follows the same central charge $c = 3.0$.

V. QUANTUM PHASE TRANSITIONS

It is interesting to study the phase transitions between the well established topological CSL and other phases surrounding it. Continuous phase transitions from such a topologically ordered phase are of general interest as examples of unconventional quantum criticality[70,71]. Thus we attempt to establish if any of the transitions in our system are indeed continuous.

First, we consider the phase transition from the CSL to the $q = (0, 0)$ Néel phase. For $J_2 = 0.2$ on YC8 cylinder, we find the transition occurs at about $J_3 \simeq 0.2$, based upon the behavior of chiral and spin correlations in Fig. 4(b) and Fig. 5. To gauge the order of the transition, we plot in Figs. 8(a) and 8(b) the J_3 dependence of the ground-state energy and entanglement entropy for $J_2 = 0.2$ in a range spanning the $q = (0, 0)$ to CSL transition on the YC8-24 cylinder. We find that both the ground-state energy and entropy vary smoothly with J_3, indeed so smoothly that a transition cannot be identified from these data. This suggests the CSL to Néel transition may be continuous. However, we should caution that the absence of sharp features is not evidence for criticality – which in any case would be difficult to verify on the small systems studied here. It does indicate that the CSL to Néel transition is not strongly first order.

This is in contrast to the transition from the CSL to the *cuboc1* phase. As shown in Figs. 8(c) and 8(d) of the results on XC8 cylinder for $J_2 = 0.2$, we find both the energy and the entropy have a sharp change at $J_3 \simeq 0.38$, which are also observed on YC8 cylinder at $J_3 \simeq 0.4$. Note that for a large system, the theoretical expectation at a first order transition between these two phases is a slope discontinuity in the ground state energy and a jump in the entanglement entropy, both of which are compatible with Figs. 8(c) and 8(d). The sharp changes observed in these quantities are also consistent with the sudden drop of chiral correlation in Fig. 4(b) as well as the enhancement of spin correlations in Fig. 6(b). All these results indicate a strong first-order transition from the CSL to the *cuboc1* phase. The first order nature of this transition is another indication that the CSL phase should not be regarded as a quantum fluctuating descendent of the *cuboc1* phase, as discussed above in Sec. IV.

Next we consider the J_1-J' model with $J_2 = J_3 = J'$ to

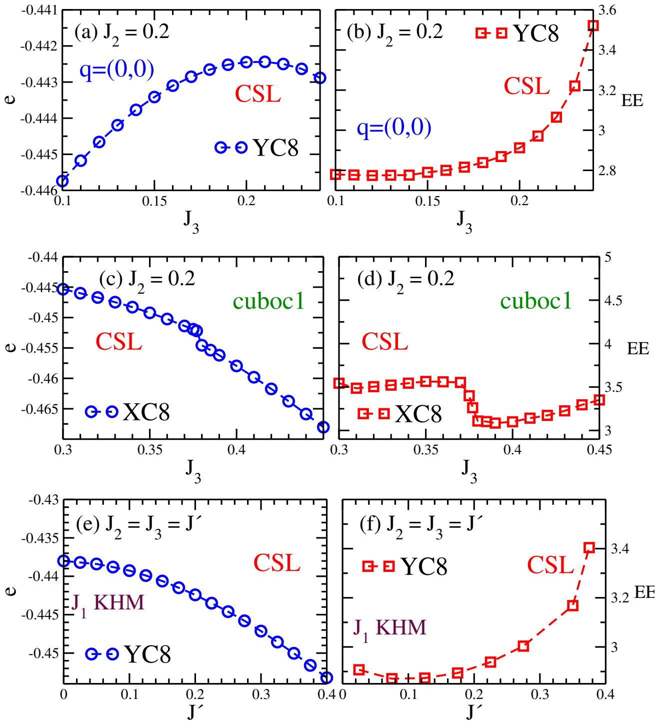

FIG. 8: Scans of ground state energy and entanglement entropy of a bipartition into equal halves, as probes of quantum phase transitions. Panels (a) and (b) show the J_3 dependence for $J_2 = 0.2$ on the YC8 cylinder over a region spanning the transition from the CSL to the $q = (0, 0)$ Néel phase. No sharp features are observed, suggesting a continuous phase transition. In panels (c) and (d) the same quantities are shown for for $J_2 = 0.2$ on the XC8 cylinder, to probe the transition from the CSL to the *cuboc1* phase. In this case an abrupt feature is observed, suggesting a first order transition. In the final two panels, (e) and (f), the system is scanned with $J_2 = J_3 = J'$ on the YC8 cylinder, to study the transition from the time-reversal invariant QSL to the CSL. In this case, the transition again appears continuous.

investigate the transition from the CSL to QSL ground state of the pure nearest-neighbor KHM. The latter phase itself is under debate, and may be a gapped Z_2 QSL[41] or a gapless QSL[56] of either Z_2 or $U(1)$ type[45,46]. By studing the chiral correlations, the transition point is determined to be $J' \simeq 0.07$ as shown in Fig. 1(a). In Figs. 8(e) and 8(f), we find that both the energy and entropy appear smooth as a function of J', leaving open the possibility of a continuous transition of the nearest-neighbor QSL state into the CSL phase[55,69].

VI. SUMMARY AND DISCUSSION

We have studied the competing quantum phases of the spin-$1/2$ J_1-J_2-J_3 KHM for $0 \leq J_2 \leq 0.25$ and $0.0 \leq J_3 \leq 1.0$ by DMRG simulations. As shown in Fig. 1(a), we find five phases: a time-reversal symmetric QSL state continuously connected to that of the nearest-neighbor Heisenberg model, a $q = (0, 0)$ Néel phase, a chiral spin liquid (CSL) phase, a non-coplanar *cuboc1* phase, and an apparent VBC phase. The CSL phase seems to arise as a result of quantum fluctuations around the line of classical degeneracy between the two types of classical order: the $q = (0, 0)$ Néel phase and *cuboc1* phase. The chirality structure of the CSL and *cuboc1* phases are distinctly different, and indeed we find a strong first order phase transition between them.

Both the quantum phase transition between the CSL and the $q = (0, 0)$ Néel state, and that between the CSL and the time-reversal symmetric QSL, are quite smooth and consistent with continuous behavior. If continuous, these could be interesting examples of unconventional quantum critical points[70,71]. It is not clear even what to expect for the universal field theories for these phase transitions from the theory of QSLs. The nature of the time-reversal symmetric QSL itself is controversial, making it hard to speak definitively about that transition. If we suppose that the QSL itself is of the gapless U(1) Dirac type[45], then this transition could be understood as simple "chiral symmetry breaking"-type transition in which a scalar mass gap appears for the Dirac fermions[58,72]. The mechanism for generation of an appropriate Chern-Simons term to describe the universal aspects of the CSL from such a Dirac mass is well-known[58,73]. However, it is not clear that the proposed U(1) Dirac state is even stable as a phase. At this point, we have only some speculative ideas for the field theories that might describe transitions from a Z_2 version of the time-reversal symmetric QSL liquid state, or from the $q = (0, 0)$ Néel state, to the CSL. We suggest this may be a possibly fruitful problem for future research.

We did not concentrate much in this work on the tentatively identified VBC phase, which occurs in the small J_2 region ($J_2 < 0.05$) as shown in Fig. 1. In this region, our DMRG calculations converge to a ground state with non-uniform bond energy, as shown in Fig. 2(d). On the XC8 cylinder, this pattern does not appear to break the lattice translational symmetry, but clearly breaks some point group symmetries of the kagomé lattice. A similar VBC pattern is also found on the XC12 cylinder[74], though there may be some suggestions of translational symmetry breaking in that case. Since a topologically trivial gapped state is not possible without an even number of spins per unit cell, the breaking of translational symmetry is a key which must be established. In the future, it will be interesting to address this issue with more care, and to compare this VBC phase to the one found in the J_1-J_2 kagome Heisenberg model with small negative second neighbor exchage, $J_2 \sim -0.05$[50].

We acknowledge useful discussions and correspondence with L. Messio, W. J. Hu, T. Grover, S. Sachdev, Z. Y. Weng, and X. G. Wen. This research is supported by the National Science Foundation through grants DMR-1408560 (S.S.G.), DMR-1206809 (L.B.), and the U.S. Department of Energy, Office of Basic Energy Sciences under grant No. DE-FG02-06ER46305 (D.N.S,W.Z.).

Note added.—Upon finalizing the manuscript we noticed a recent preprint reporting a DMRG[75] study of the J_1-J_2 Heisenberg model, and also finds that the $q = (0, 0)$ order emerges for $J_2 > 0.2$. We also noticed a preprint on variational Monte Carlo studies[76] of the same model based on the

Gutzwiller projected fermion wavefunction, which claims that the $U(1)$ Dirac spin liquid may be stable in a region with finite $J_2 > 0$.

[1] L. Balents, Nature **464**, 199 (2010).
[2] X. G. Wen, Phys. Rev. B *40*, 7387 (1989).
[3] X. G. Wen and Q. Niu, Phys. Rev. B *41*, 9377 (1990).
[4] X. G. Wen, Int. J. Mod. Phys. B **4**, 239 (1990).
[5] P. W. Anderson, Science **235**, 1196 (1987).
[6] P. A. Lee, N. Nagaosa, and X. G. Wen, Rev. Mod. Phys. **78**, 17 (2006).
[7] P. A. Lee, Science **321**, 1306 (2008).
[8] X. G. Wen, Phys. Rev. B **44**, 2664 (1991).
[9] T. Senthil and M.P.A. Fisher, Phys. Rev. B **62**, 7850 (2000); Phys. Rev. Lett. **86**, 292 (2001).
[10] D. S. Rokhsar and S. A. Kivelson, Phys. Rev. Lett. **61**, 2376 (1988).
[11] R. Moessner and S. L. Sondhi, Phys. Rev. Lett. **86**, 1881 (2001).
[12] L. Balents, M. P. A. Fisher, and S. M. Girvin, Phys. Rev. B **65**, 224412 (2002).
[13] T. Senthil and O. Motrunich, Phys. Rev. B **66**, 205104 (2002).
[14] D. N. Sheng and L. Balents, Phys. Rev. Lett. **94**, 146805 (2005).
[15] A. Kitaev, Ann. Phys. (N.Y.) **321**, 2 (2006).
[16] S. V. Isakov, M. B. Hastings, R. G. Melko, Nat. Phy. **7**, 772 (2011).
[17] H. Yao and S. A. Kivelson, Phys. Rev. Lett. **99**, 247203 (2007).
[18] P. Mendels, F. Bert, M. A. de Vries, A. Olariu, A. Harrison, F. Duc, J. C. Trombe, J. S. Lord, A. Amato, and C. Baines, Phys. Rev. Lett. **98**, 077204 (2007).
[19] J. S. Helton, K. Matan, M. P. Shores, E. A. Nytko, B. M. Bartlett, Y. Yoshida, Y. Takano, A. Suslov, Y. Qiu, J.-H. Chung, D. G. Nocera, and Y. S. Lee, Phys. Rev. Lett. **98**, 107204 (2007).
[20] M. A. de Vries, J. R. Stewart, P. P. Deen, J. Piatek, G. Nilsen, H. M. Rnnow, and A. Harrison, Phys. Rev. Lett. **103**, 237201 (2009).
[21] D. Wulferding, P. Lemmens, P. Scheib, J. Röder, P. Mendels, S. Chu, T. Han, and Y. S. Lee, Phys. Rev. B **82**, 144412 (2010).
[22] B. Fåk, E. Kermarrec, L. Messio, B. Bernu, C. Lhuillier, F. Bert, P. Mendels, B. Koteswararao, F. Bouquet, J. Ollivier, A. D. Hillier, A. Amato, R. H. Colman, and A. S. Wills, Phys. Rev. Lett. **109**, 037208 (2012).
[23] T. H. Han, J. S. Helton, S. Chu, D. G. Nocera, J. A. Rodriguez-Rivera, C. Broholm, and Y. S. Lee, Nature **492**, 7429 (2012).
[24] L. Clark, J. C. Orain, F. Bert, M. A. De Vries, F. H. Aidoudi, R. E. Morris, P. Lightfoot, J. S. Lord, M. T. F. Telling, P. Bonville, J. P. Attfield, P. Mendels, and A. Harrison, Phys. Rev. Lett. **110**, 207208 (2013).
[25] Y. Shimizu, K. Miyagawa, K. Kanoda, M. Maesato, and G. Saito, Phys. Rev. Lett. **91**, 107001 (2003).
[26] Y. Kurosaki, Y. Shimizu, K. Miyagawa, K. Kanoda, and G. Saito, Phys. Rev. Lett. **95**, 177001 (2005).
[27] T. Itou, A. Oyamada, S. Maegawa, M. Tamura, and R. Kato, Phys. Rev. B **77**, 104413 (2008).
[28] B. Bernu, C. Lhuillier, and L. Pierre, Phys. Rev. Lett. **69**, 2590 (1992).
[29] O. I. Motrunich, Phys. Rev. B **72**, 045105 (2005).
[30] M. Q. Weng, D. N. Sheng, Z. Y. Weng, and R. J. Bursill, Phys. Rev. B **74**, 012407 (2006).
[31] O. A. Starykh and L. Balents, Phys. Rev. Lett. **98**, 077205 (2007).
[32] F. Wang, Phys. Rev. B **82**, 024419 (2010).
[33] Y. M. Lu and Y. Ran, Phys. Rev. B **84**, 024420 (2011).
[34] R. Ganesh, J. van den Brink, and S. Nishimoto, Phys. Rev. Lett. **110**, 127203 (2013).
[35] Z. Y. Zhu, D. A. Huse, and S. R. White, Phys. Rev. Lett. **110**, 127205 (2013).
[36] S. S. Gong, D. N. Sheng, O. I. Motrunich, and M. P. A. Fisher, Phys. Rev. B **88**, 165138 (2013).
[37] N. Read and S. Sachdev, Phys. Rev. Lett. **66**, 1773 (1991).
[38] H. C. Jiang, H. Yao, and L. Balents, Phys. Rev. B **86**, 024424 (2012).
[39] S. S. Gong, W. Zhu, D. N. Sheng, O. I. Motrunich, and M. P. A. Fisher, Phys. Rev. Lett. **113**, 027201 (2014).
[40] H. C. Jiang, Z. Y. Weng, and D. N. Sheng, Phys. Rev. Lett. **101**, 117203 (2008).
[41] S. Yan, D. Huse, and S. R. White, Science **332**, 1173 (2011).
[42] S. Depenbrock, I. P. McCulloch, and U. Schollwöck, Phys. Rev. Lett. **109**, 067201 (2012).
[43] H. C. Jiang, Z. H. Wang, and L. Balents, Nat. Phy. **8**, 902 (2012).
[44] S. Nishimoto, N. Shibata, and C. Hotta, Nat. Commu. **4**, 2287 (2013).
[45] Y. Ran, M. Hermele, P. A. Lee, and X. G. Wen, Phys. Rev. Lett. **98**, 117205 (2007).
[46] Y. Iqbal, F. Becca, S. Sorella, and D. Poilblanc, Phys. Rev. B **87**, 060405(R) (2013).
[47] Y. Iqbal, D. Poilblanc, and F. Becca, Phys. Rev. B **89**, 020407(R) (2014).
[48] T. Tay and O. I. Motrunich, Phys. Rev. B **84**, 020404(R) (2011).
[49] P. Sindzingre and C. Lhuillier, Europhys. Lett. **88**, 27009 (2009).
[50] S. Yan, D. A. Huse, and S. R. White, Bulletin of the American Physical Society (2012).
[51] R. Suttner, C. Platt, J. Reuther, and R. Thomale, Phys. Rev. B **89**, 020408 (2014).
[52] Y. C. He, D. N. Sheng, and Y. Chen, Phys. Rev. B **89**, 075110 (2014).
[53] S. S. Gong, W. Zhu, and D. N. Sheng, Sci. Rep. **4**, 6317 (2014).
[54] Y. C. He, D.N. Sheng, and Y. Chen, Phys. Rev. Lett. **112**, 137202 (2014).
[55] Y. C. He and Y. Chen, Phys. Rev. Lett. **114**, 037201 (2015).
[56] W. Zhu, S. S. Gong, and D. N. Sheng, arXiv:1410.4883.
[57] V. Kalmeyer and R. B. Laughlin, Phys. Rev. Lett. **59**, 2095 (1987).
[58] X. G. Wen, F. Wilczek, and A. Zee, Phys. Rev. B **39**, 11413 (1989).
[59] J. W. Mei and X. G. Wen, arXiv:1407.0869.
[60] W. J. Hu, W. Zhu, Y. Zhang, S. S. Gong, F. Becca, and D. N. Sheng, arXiv:1411.1327.
[61] B. Bauer, L. Cincio, B. P. Keller, M. Dolfi, G. Vidal, S. Trebst, and A. W. W. Ludwig, Nat. Commu. **5**, 5137 (2014).
[62] S. R. White, Phys. Rev. Lett. **69**, 2863 (1992).
[63] L. Messio, B. Bernu, and C. Lhuillier, Phys. Rev. Lett. **108**, 207204 (2012).
[64] I. P. McCulloch and M. Gulácsi, Europhys. Lett. **57**, 852 (2002); I. P. McCulloch, J. Stat. Mech. **2007**, P10014 (2007).
[65] While the calculations for $L = 2, 4$ are easy to converge, we find that m^2 continues to grow with increasing kept states for $L = 6$. By keeping the states up to about 24000, the increase of m^2 is negligible and the results are close to convergence.
[66] O. Janson, J. Richter, and H. Rosner, Phys. Rev. Lett. **101**, 106403 (2008); J. Phys. Conf. Ser. **145**, 012008 (2009).
[67] A. Altland, and B. D. Simons, *Condensed matter field theory*, Cambridge University Press, 2010.

[68] P. Calabrese and J. Cardy, J. Stat. Mech.: Theor. Exp. P06002 (2004).
[69] M. Barkeshli, arXiv:1307.8194.
[70] T. Senthil, A. Vishwanath, L. Balents, S. Sachdev, and M. P. A. Fisher, Science **303**, 1490 (2004).
[71] T. Senthil, L. Balents, S. Sachdev, A. Vishwanath, and M. P. A. Fisher, Phys. Rev. B **70**, 144407 (2004).
[72] M. Hermele, T. Senthil, and M. P. A. Fisher, Phys. Rev. B **72**, 104404 (2005).
[73] A. N. Redlich, Phys. Rev. D **29**, 2366 (1984).
[74] On the XC12 cylinder, while the bond energy we obtained keeps breaking the lattice rotational symmetry as that on the XC8 cylinder in Fig. 2(d), it also has a slightly translational symmetry breaking, which may be owing to the less convergence.
[75] F. Kolley, S. Depenbrock, I. P. McCulloch, U. Schollwöck, and V. Alba, arXiv:1410.7911.
[76] Y. Iqbal, D. Poilblanc, F. Becca, Phys. Rev. B **91**, 020402(R) (2015).